PROCEEDINGS of the
23rd International Congress on Acoustics

9 to 13 September 2019 in Aachen, Germany

Acoustic scattering in arrays of orifices, slits and tube rows with mean flow: A comparison

Charles BOAKES; Aswathy SURENDRAN*; Dong YANG; Aimee MORGANS

Imperial College London, United Kingdom

Abstract

Thermoacoustic oscillations result from positive feedback between acoustic fluctuations and unsteady heat transfer into or out of the system. The thermoacoustic response of combustion system heat exchangers in cross flow is assumed to be dominated by two effects: acoustic scattering at the heat exchanger tube row and unsteady heat transfer from the tube row. While the latter causes a significant reduction in the net energy of the oscillations, the influence of both the effects on the acoustic fluctuations needs to be addressed carefully to predict the thermoacoustic response of the heat exchanger. To this end, we adopt a sequential approach where the acoustic scattering and the heat transfer are assumed to be independent of each other. In the present work, we focus on the acoustic scattering behaviour of heat exchanger tubes (only) by comparing existing acoustic models for orifices, slits and tube rows and identifying those operating regimes where the different models are valid and overlap. This will enable us to formulate appropriate acoustic models for the various operating regimes of the heat exchanger tube rows.

Keywords: Acoustic scattering, Heat exchangers, Aeroacoustic models

1. INTRODUCTION

The present work is motivated by the use of heat exchangers in futuristic aero-propulsion engines (1). Heat exchangers, much like flames and other heat sources, can influence the thermoacoustic behaviour of combustion systems that include them. Their behaviour is assumed to be dominated by two effects: acoustic scattering at the heat exchanger tube row and the unsteady heat transfer across the tube row. It is therefore crucial to accurately model these two effects. The present work is dedicated to the acoustic scattering effect of heat exchanger tube rows.

Heat exchanger tubes are typically circular in cross-section, but can also be approximated by thin plates of rectangular cross section, separated by a rectangular gap. Studies conducted with the latter configuration have shown to have a stabilising influence on combustion systems undergoing thermoacoustic instabilities (2). There exists vast literature for the acoustic modelling of slits and perforated plates (3), and in the present work, we focus only on three existing models: a Quasi-steady cylinder model applied to an array of cylindrical tubes, the Dowling and Hughes slit model applied to rectangular slits and the modified Cummings slit model adapted for a tube row. The predictions of the acoustic scattering matrices from these models are compared in order to establish their validity in different operating regimes of the heat exchanger tube rows.

The structure of the paper is as follows: the three existing models are described in Section 2. In Section 3, we compare the acoustic scattering matrix predictions from the three models and draw our preliminary conclusions in Section 4.

2. ACOUSTIC MODELS

The flow past heat exchanger tubes in cross flow is essentially flow through a gap or constriction. This produces a jet and an associated shear layer downstream of the gap. When a low frequency acoustic wave is introduced

* Corresponding author: a.surendran@imperial.ac.uk

into the system, it creates high frequency evanescent waves and low frequency planar waves. Typically, the evanescent waves decay faster than the planar waves, and are hence found closer to the gap. Farther from the constriction, we have only low frequency planar waves that are one dimensional. Moreover, in most of the combustion systems undergoing thermoacoustic instabilities, the frequency range of interest is generally $\sim \mathcal{O}(100)$Hz. Therefore, in the present study, we restrict our analysis to low frequency planar 1-D waves. To enable us to develop a 1-D model for the aeroacoustic behaviour of heat exchangers, we compare the following existing models which account differently for the gap shape.

- A Quasi-steady model developed for a row of cylinders (Section 2.1)
- The Dowling and Hughes model for thin slits (Section 2.2)
- The modified Cummings model developed for thin slits and applied to tube rows (Section 2.3)

2.1 Quasi-steady cylinder model

The schematic of the tube row geometry considered is illustrated in Figure 1. It consists of two half cylinders placed inside a duct of height h_d and having a bias flow of velocity u_g through the gap of height h_g between the cylinders. The bias flow then forms a jet of height h_j downstream of the cylinder. It is sufficient to model this system instead of an array of cylinders as they are equivalent (through the method of image sources).

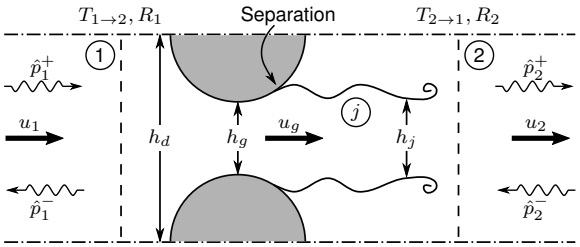

Figure 1. Schematic for the flow domain in the Quasi-steady cylinder model

The quasi-steady model developed for tube rows can be found in Surendran et al. (4). This approach, first proposed by Ronneberger (5), assumes that the time-dependent acoustic perturbations of the flow are sufficiently slow such that the unsteady terms in the relevant 1-D conservation equations can be neglected. This is valid for small Strouhal numbers $(St = \omega d/u)$ and small Helmholtz numbers $(He = \omega d/c)$, where ω is the angular frequency, d is the diameter of the tube, u is the velocity and c is the speed of sound. The latter requires that the acoustic wavelength is much larger than the tube diameter, leading to a *compact* tube row assumption. It is also assumed that the acoustic wavelength is much larger than the mixing zone downstream of the tube row. Consequently, no phase changes in the acoustic scattering properties are expected across the tube row.

The duct is divided into three regions: Region 1, region j and region 2. Region 1 and 2 have uniform flows and are upstream and downstream of the cylinders, respectively. Region j lies between regions 1 and 2 and contains the cylinders, the jet and the mixing region. Assuming isentropic and irrotational flow between the regions 1 and j, the conservation of mass and energy under the assumptions of quasi-steadiness and perfect gas behaviour can be applied. This yields Eqs. (1)-(3), where the variables ρ, p and γ denote the density, pressure and ratio of specific heats, respectively, while the subscripts indicate the corresponding regions.

$$h_d \rho_1 u_1 = h_j \rho_j u_j \qquad \text{(continuity)} \tag{1}$$

$$\frac{1}{2}u_1^2 + \frac{\gamma}{\gamma-1}\frac{p_1}{\rho_1} = \frac{1}{2}u_j^2 + \frac{\gamma}{\gamma-1}\frac{p_j}{\rho_j} \qquad \text{(energy)} \tag{2}$$

$$\frac{p_1}{p_j} = \left(\frac{\rho_1}{\rho_j}\right)^{\gamma} \qquad \text{(isentropic)} \tag{3}$$

Downstream of the mixing region, the flow is uniform and non-isentropic. Hence, the conservation of mass and momentum are used to link regions j and 2 as shown in Eqs. (4)-(5). Neglecting heat transfer, viscous and frictional losses at the wall, conservation of energy can be applied across regions 1 and 2 as given in Eq. (6).

$$h_j \rho_j u_j = h_d \rho_2 u_2 \qquad \text{(continuity)} \tag{4}$$

$$h_d p_j + h_j \rho_j u_j^2 = h_d p_2 + h_d \rho_2 u_2^2 \qquad \text{(momentum)} \tag{5}$$

$$\frac{1}{2}u_1^2+\frac{\gamma}{\gamma-1}\frac{p_1}{\rho_1}=\frac{1}{2}u_2^2+\frac{\gamma}{\gamma-1}\frac{p_2}{\rho_2}\qquad\text{(energy)}\tag{6}$$

These equations (Eqs. (1)-(6)) are then linearised about a mean condition by decomposing u, p and ρ into the sum of a mean component ($\bar{}$) and a small acoustic perturbation component ($'$), while neglecting higher order terms of the primed quantities (6). These decompositions are shown in Eq. (7) and the derivation of the linearised equations can be found in Appendix D of (7). The acoustic perturbations are related to the complex amplitudes of the forward and backward travelling pressure waves $\hat{p}^+_{1,2}$ and $\hat{p}^-_{1,2}$ as shown in Eq. (8), where s' is the entropy perturbation, c_p is the specific heat at constant pressure and the subscript i denote the region. Substituting these expressions for the velocity, pressure and density perturbations yields a set of equations in terms of $\hat{p}^{\pm}_{1,2}$ that can be manipulated to form a scattering matrix. In the absence of an incoming entropy wave ($s'_1=0$), the scattering matrix will be of the form shown in Eq. (9). Here, $T_{1\to2}$ and R_1 are the transmission and reflection coefficients for a wave incident from upstream and $T_{2\to1}$ and R_2 are the transmission and reflection coefficients for a wave incident from downstream.

$$p=\bar{p}+p' \qquad u=\bar{u}+u' \qquad \rho=\bar{\rho}+\rho'\tag{7}$$

$$p'_i=\hat{p}^+_i+\hat{p}^-_i \qquad u'_i=\frac{\hat{p}^+_i-\hat{p}^-_i}{\bar{\rho}_i c_i} \qquad \rho'_i=\frac{\hat{p}^+_i+\hat{p}^-_i}{c_i^2}-\frac{\bar{\rho}_i}{c_p}s'_i\tag{8}$$

$$\begin{bmatrix}\hat{p}^+_2\\ \hat{p}^-_1\end{bmatrix}=\begin{bmatrix}T_{1\to2} & R_2\\ R_1 & T_{2\to1}\end{bmatrix}\begin{bmatrix}\hat{p}^+_1\\ \hat{p}^-_2\end{bmatrix}\tag{9}$$

2.2 Dowling and Hughes slit model

The Dowling and Hughes model describes the acoustic scattering behaviour of thin rectangular slits with bias flow by extending the analysis of Howe (8). The flow domain, as shown in Figure 2, consists of two infinite half planes connected by the slit. The infinitely long slit plate can be approximated to the geometry shown, again through the method of image sources. Each slit has a width of h_g and is spaced h_d distance apart, having a bias flow velocity of u_g though the slits. The flow is assumed to be incompressible and hence $\bar{\rho}_1=\bar{\rho}_2=\rho_0$.

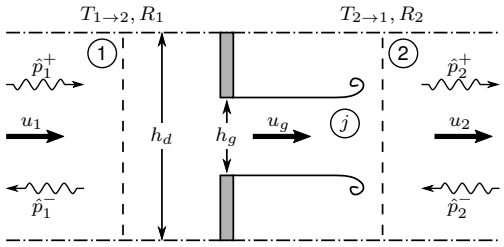

Figure 2. Schematic for the flow domain in the Dowling and Hughes slit model.

Howe (8) described the attenuation of acoustic waves incident on screens with circular perforations by assuming that the acoustic losses are due to the unsteady convection of vorticity from the hole rims. Using stagnation enthalpy $B=p'/\rho_0+\frac{1}{2}\boldsymbol{u}^2$ as the acoustic variable, the acoustic field is described using Howe's analogy (9), reducing the problem to that of solving an inhomogeneous Helmholtz equation in stagnation enthalpy (Eq. (10)).

$$(\nabla^2+k^2)B=-\nabla\cdot(\boldsymbol{\Omega'}\times\bar{\boldsymbol{u}}_{\boldsymbol{g}}),\tag{10}$$

where k is the wave number, $\boldsymbol{\Omega'}$ is the amplitude of linear vorticity perturbations generated by the incident acoustic wave, and $\bar{\boldsymbol{u}}_{\boldsymbol{g}}$ is the mean convection velocity of the shed vorticity. It is assumed that vorticity is convected without any dissipation by the mean flow, and its strength is determined by the Kutta condition.

Dowling and Hughes solved Eq. (10) in the limit of small open area ratio ($\eta=h_g/h_d$) and small Helmholtz number. They showed that the transmission and reflection coefficients can be determined by Eqs. (11) and (12),

$$T_{1\to2}=\rho_0\omega\dot{V}/(kh_d),\tag{11}$$

$$R_1=1-T_{1\to2},\tag{12}$$

with

$$\frac{\rho_0\omega\dot{V}}{kh_d}=\frac{i\pi\eta/(2StM_g)}{i\pi\eta/(2StM_g)-\ln(\pi\eta)+\ln 2/\Phi(St)},\tag{13}$$

$$\Phi(St) = 1 - \frac{1}{St \ln 2} \left\{ \frac{\pi I_0(St) e^{-St} + 2i \sinh(St) K_0(St)}{\pi e^{-St} \left[I_1(St) + \frac{I_0(St)}{St \ln 2} \right] + 2i \sinh(St) \left[\frac{K_0(St)}{St \ln 2} \right] - K_1(St)} \right\}, \tag{14}$$

where $\dot{V}$ is the perturbation volume flux through the slit, $St = \omega h_g/(2u_g)$, $M_g = \bar{u}_g/c$ is the mean Mach number of the bias flow and I_m and K_m are the modified Bessel functions of order m. Again, the scattering matrix would be of the form shown in Eq. (9).

2.3 Modified Cummings slit model

Cummings (10, 11) developed a model to describe the acoustic transmissions through duct terminations using unsteady Bernoulli's equation. The configuration studied in (10) is shown in Figure 3a, where an incompressible uniform mean flow with superimposed plane acoustic waves travels through a converging nozzle of circular cross section. The flow then separates at the nozzle exit to form a jet with height h_{vc} (*vena contracta*). The velocities at 1 and 2 can be related to the gap velocity u_g through the open area ratio η $(= h_g/h_d)$ and the contraction coefficient $\sigma = h_{vc}/h_g$ as $u_1 = \eta u_g$ and $u_2 = u_g/\sigma$. In the present study, we adapt a similar flow structure for the slit (see Figure 3b), where the uniform flow upstream of the slit separates at the slit edge forming a jet.

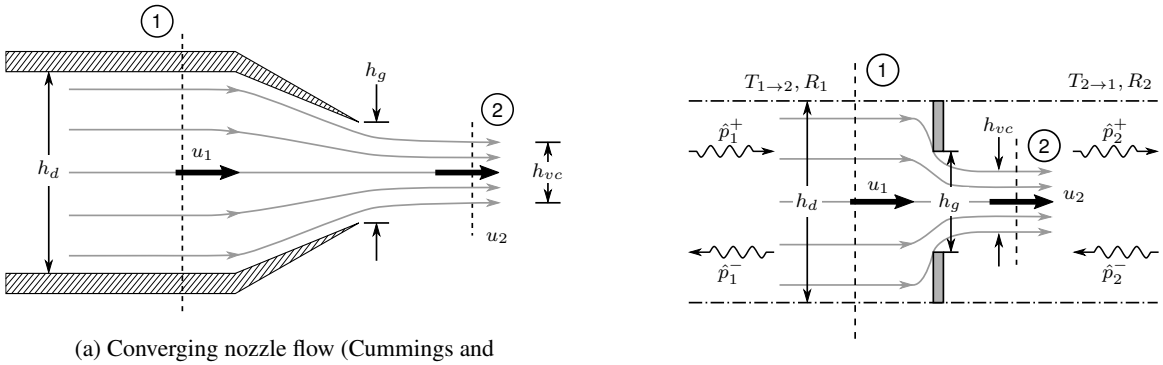

(a) Converging nozzle flow (Cummings and Eversman (10))

(b) Flow though a slit (Present study)

Figure 3. Geometry used in the modified Cummings model.

Applying unsteady Bernoulli's equation from region 1 to 2 yields

$$\int_1^2 \rho_0 \frac{du_g}{dt} dx + \frac{\rho_0}{2} \left(u_2^2 - u_1^2 \right) = p_1 - p_2. \tag{15}$$

Defining an effective length L for the slug of fluid undergoing unsteady motion at the slit as $\int_1^2 \rho_0 (du_g/dt) dx = \rho_0 L (du_g/dt)$, the Cummings equation (Eq. (15)) can be written as

$$\rho_0 L \frac{du_g'}{dt} + \rho_0 \left(\bar{u}_g + u_g' \right)^2 \frac{1 - \eta^2 \sigma^2}{2\sigma^2} = p_1 - p_2. \tag{16}$$

Cummings (11) argued that for high amplitude pressure fluctuations, the jet formed at the orifice can grow and diminish periodically due to flow reversal, causing L to vary. However, for low amplitude pressure perturbations that do not lead to flow reversal, Luong et al. (12) suggested that $L = 2l_0 + l_w$, where $l_0 \approx (\pi/4) h_g$ is the end correction contributed by the duct termination with irrotational flow on one side and l_w is the thickness of the orifice. Subtracting the steady contribution from Eq. (16), and for small η, one can obtain the equation for perturbations as (12)

$$(2l_0 + l_w) \frac{du_g'}{dt} + \frac{u_g'}{\sigma^2} \left(\bar{u}_g + \frac{u_g'}{2} \right) = \frac{p_I}{\rho_0}, \tag{17}$$

where $p_I = p_1' - p_2'$. Albaharna (13) linearised Eq. (17) by neglecting the higher order terms i.e., products of perturbation terms, and evaluated the transmission and reflection coefficients. This linearised equation (Eq. (18)) is referred to as the *modified Cummings model* in the present paper.

$$(2l_0 + l_w) \frac{du_g'}{dt} + \frac{u_g' \bar{u}_g}{\sigma^2} = \frac{p_I}{\rho_0} \tag{18}$$

Manipulating the results in (13) for an acoustic wave incident from the upstream side with temporal variation $e^{i\omega t}$ (see Figure 3b), we obtain the transmission and reflection coefficients as

$$T_{1\to2} = \frac{2}{1+\eta M_g}\left(\frac{4i\beta StM_g^2 + (M_g/\sigma)^2 + 1}{4i\beta StM_g/\eta + M_g/(\eta\sigma^2) + 2/(1+\eta M_g)}\right), \tag{19}$$

$$R_1 = \left(\frac{4i\beta StM_g/\eta + M_g/(\eta\sigma^2)}{4i\beta StM_g/\eta + M_g/(\eta\sigma^2) + 2/(1+\eta M_g)}\right), \tag{20}$$

where $St = \omega h_g/(2u_g)$ and β is the end correction coefficient. Albaharna used $\sigma = 0.75$ as suggested and experimentally validated by Cummings (11), and used the end correction model for rectangular perforations suggested in (14), to define β. However, this model does not hold for situations where the slit length $\gg$ slit width as β becomes infinite. Therefore, in the present study, we use the end correction for a rectangular orifice in a baffle wall as given in (15) i.e.,

$$\beta = \frac{l_0}{h_g} = \frac{1}{\pi}\ln\left[\frac{1}{2}\tan\left(\frac{\pi\eta}{4}\right) + \frac{1}{2}\cot\left(\frac{\pi\eta}{4}\right)\right] \tag{21}$$

3. RESULTS FOR MODEL COMPARISONS

The transmission, reflection and absorption coefficients for the different models (and their corresponding geometries) are compared in this section. The absorption coefficient (α) is defined as the ratio of the acoustic energy absorbed to the acoustic energy incident (16). Across any two regions denoted by 1 and 2, $\alpha_{1\to2}$ can be expressed as

$$\alpha_{1\to2} = 1 - \left[\frac{|\hat{p}_1^-|^2(1-M_1)^2 + |\hat{p}_2^+|^2(1+M_2)^2(\bar{\rho}_1 c_1/\bar{\rho}_2 c_2)\mathscr{A}_2/\mathscr{A}_1}{|\hat{p}_1^+|^2(1+M_1)^2 + |\hat{p}_2^-|^2(1-M_2)^2(\bar{\rho}_1 c_1/\bar{\rho}_2 c_2)\mathscr{A}_2/\mathscr{A}_1}\right], \tag{22}$$

where $\mathscr{A}$ is the area of cross section. For the analysis provided in this paper, we have used the system properties shown in Table 1. Here, d is the diameter of the cylinder and μ is the dynamic viscosity.

Table 1. System properties

Property	Unit	Value	Property	Unit	Value
d	[m]	0.02	μ	[Pa s]	1.8×10^{-5}
ρ	[kg/m^3]	1.2	η	-	0.1
c	[m/s]	700	γ	-	1.4

Figure 4 shows the coefficients predicted by the three models for various excitation frequencies (in terms of the St), $M_g = 0.1$ and $\eta = 0.1$. The Dowling and Hughes model (D&H) and the modified Cummings model (MC) are for rectangular slits and the Quasi-steady model (QS) is for tube rows. It can be observed that the D&H and MC models are consistent and exhibit similar behaviour in frequency, whereas the QS model, experimentally validated in (4), does not exhibit any dependence on frequency. It can also be noted that at very low Strouhal numbers ($St \leq 0.4$), the D&H and MC models also predict quasi-steady behaviour, reinforcing the low Strouhal and low Helmholtz numbers assumptions used in the QS model for similar flow and geometry considerations. However, the QS model predicts a higher transmission and lower reflection and absorption coefficients compared to the other two models.

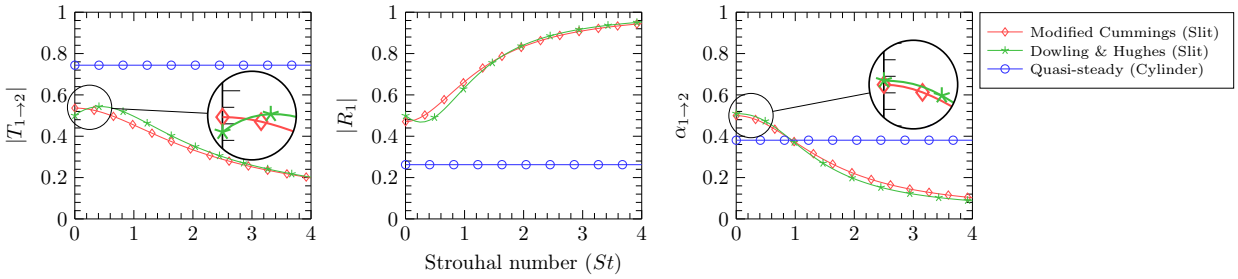

Figure 4. Transmission, reflection and absorption coefficients for an upstream perturbation for $M_g = 0.1$ and $\eta = 0.1$.

The predictions of the different models for a given frequency such that $St \to 0$ ($= 10^{-6}$), $\eta = 0.1$ and for various gap Mach number M_g are shown in Figure 5. Though the overall trend exhibited by the different coefficients are similar, the QS model is seen to again predict higher transmission and lower reflection coefficients for lower M_g values. For the transmission coefficient, as M_g increases, the MC model is seen to diverge from the D&H model, though the reflection and absorption coefficients are consistent. Since the QS model has been experimentally verified for tube rows (4) and the D&H model has been experimentally verified for plates with slits (6), it can be concluded that tube rows cannot be approximated as rectangular slits as was proposed in (13).

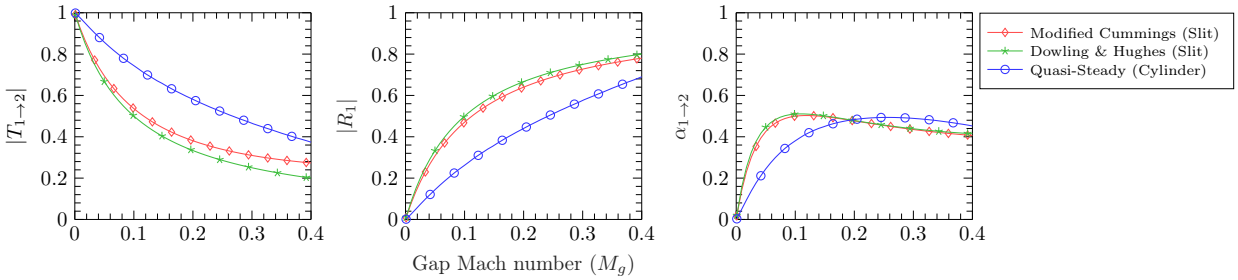

Figure 5. Transmission, reflection and absorption coefficients for an upstream perturbation for $St \to 0$ and $\eta = 0.1$.

The discrepancy between the predictions of the QS and MC models can be explained by the different incompressible steady flow loss coefficients implied by Eq. (5) and Eq. (16). The loss coefficient defined as

$$K = \frac{\Delta p_0}{0.5 \rho_0 u_g^2}, \tag{23}$$

and applied to the QS and MC models give

$$K_{QS} = (1 - \eta_j)^2, \tag{24}$$

$$K_{MC} = \left(\frac{1}{\sigma^2} - \eta^2 \right). \tag{25}$$

where $\eta_j = h_j / h_d$. Since η, η_j and σ are less than 1, $K_{MC} > K_{QS}$, demonstrating that the MC model implies a greater loss or dissipation than the QS model. If we treat σ or the contraction coefficient as an arbitrary quantity, K_{MC} can be matched with K_{QS} or any other given loss coefficient. The effect of this matching is depicted in Figure 6 and 7, where the low Strouhal limit of the MC model now coincides with the QS model. In Figure 7, the small deviation between the two models at higher Mach numbers may be due to the different linearised forms of Eqs. (5) and (16). Such an adjustment might allow the use of the MC model to tube rows, provided an appropriate end correction is applied.

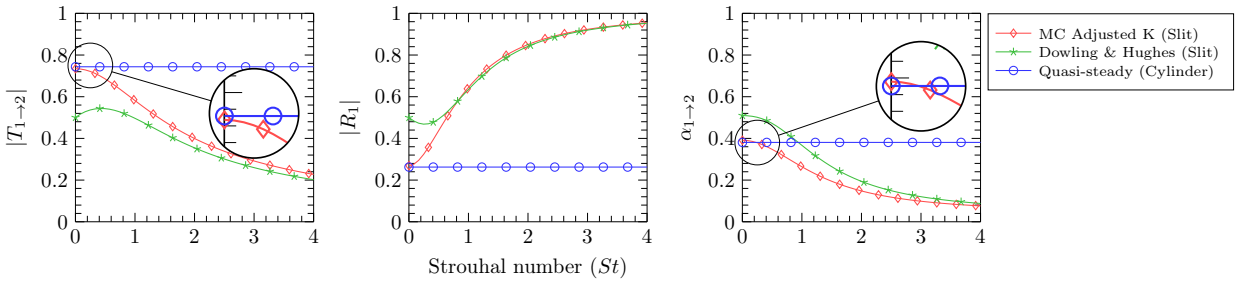

Figure 6. Transmission, reflection and absorption coefficients for an upstream perturbation for $M_g = 0.1$ and $\eta = 0.1$. The contraction coefficient in the modified Cummings model is adjusted to match K_{MC} with K_{QS}.

4. CONCLUSIONS

In order to describe the acoustic scattering behaviour of heat exchanger tube rows, we considered three existing models: the Quasi-steady cylinder model applied to tube rows, the Dowling and Hughes slit model applied

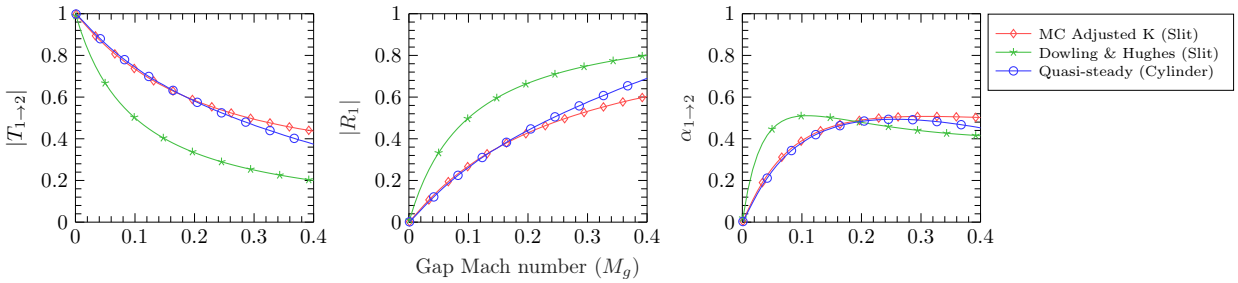

Figure 7. Transmission, reflection and absorption coefficients for an upstream perturbation for $St \to 0$ and $\eta = 0.1$. The contraction coefficient in the modified Cummings model is adjusted to match K_{MC} with K_{QS}.

to rectangular slits and the modified Cummings slit model. The predictions for the transmission, reflection and absorption coefficients for the three models show that the slit models are more dissipative than the tube row model, indicating that heat exchanger tube rows cannot be approximated as rectangular slits. However, predictions from the modified Cummings model, corrected for the incompressible steady flow loss coefficient, gave better agreement with the results of the Quasi-steady model, for low Strouhal and Helmholtz numbers. One of the advantages of using such a corrected loss coefficient approach is that this information is readily available through empirical correlations or from steady CFD simulations, for most geometries widely used in engineering applications, and hence can be easily incorporated into the MC model. Presently, studies are being undertaken to extend the approach given in this paper to accommodate heat transfer in the flow domain.

ACKNOWLEDGEMENTS

We gratefully acknowledge the financial support from the European Research Council Grant AFIRMATIVE (2018-23). We also acknowledge the technical inputs and discussions undertaken with Dr. Ignacio Duran, Reaction Engines Limited, U. K.

REFERENCES

[1] Reaction Engines Limited. [Online] available: http://www.reactionengines.co.uk/.

[2] Surendran, A.; Heckl, M. A. Passive instability control by a heat exchanger in a combustor with nonuniform temperature. International Journal of Spray and Combustion Dynamics, Vol 9 (4), 2017, pp 380-393.

[3] Lahiri, C.; Bake, F. A review of bias flow liners for acoustic damping in gas turbine combustors. Journal of Sound and Vibration, Vol 400, 2017, pp 564–605.

[4] Surendran, A.; Heckl, M. A.; Peerlings, L.; Boij, S.; Bodén, H.; Hirschberg, A. Aeroacoustic response of an array of tubes with and without bias-flow. Journal of Sound and Vibration, Vol 434, 2018, pp 1-16.

[5] Ronneberger, D. Experimentelle Untersuchungen zum akustischen Reflexionsfaktor von unstetigen Querschnittsänderungen in einem luftdurchströmten Rohr. Acustica, Vol 19, 1967/68, pp 222-235 .

[6] Dowling, A. P.; Stow, S. R. Acoustic Analysis of Gas Turbine Combustors. Journal of Propulsion and Power, Vol 19 (5), 2003, pp 751-764.

[7] Surendran, A. Passive control of thermoacoustic instabilities in idealised combustion systems using heat exchangers. PhD Thesis, Keele University, 2017.

[8] Howe, M. S. On the Theory of Unsteady High Reynolds Number Flow Through a Circular Aperture. Proceedings of the Royal Society A: Mathematical, Physical and Engineering Sciences, Vol 366 (1725), 1979, pp 205-223.

[9] Howe, M. S. Acoustics of Fluid-Structure Interactions. Cambridge University Press, Cambridge (UK), 1st edition, 1998.

[10] Cummings, A.; Eversman, W. High amplitude acoustic transmission through duct terminations: Theory. Journal of Sound and Vibration, Vol 91 (4), 1983, pp 503-518.

[11] Cummings, A. Transient and multiple frequency sound transmission through perforated plates at high amplitude. The Journal of the Acoustical Society of America, Vol 79 (4), 1986, pp 942-951.

[12] Luong, T.; Howe, M. S.; McGowan, R. S. On the Rayleigh conductivity of a bias-flow aperture. Journal of Fluids and Structures, Vol 21, 2005, pp 769-778.

[13] Albaharna, A. Thermoacoustic Instabilities in Pre-Burners of Hybrid Rocket Engines. MEng Thesis, Imperial College London, 2018.

[14] Vigran, T. E. The acoustic properties of panels with rectangular apertures. The Journal of the Acoustical Society of America, Vol 135 (5), 2014, pp 2777-2784.

[15] Mechel, F. P. Formulas of Acoustics. Springer-Verlag, Heidelberg (Germany), 2nd edition, 2008.

[16] Morfey, C. L. Sound transmission and generation in ducts with flow. Journal of Sound and Vibration, Vol 14 (1), 1971, pp 37-55.